

# Preparation and characteristics study of nano-porous silicon UV photodetector

Raid A. Ismail<sup>1</sup> · Alwan M. Alwan<sup>1</sup> · Ahmed S. Ahmed<sup>1</sup>

Received: 14 March 2016 / Accepted: 19 December 2016 / Published online: 26 December 2016  
© The Author(s) 2016. This article is published with open access at Springerlink.com

**Abstract** In this study, influence of rapid thermal oxidation RTO and embedding of gold nanoparticles on the performance of porous silicon photodetector synthesised by anodization technique were investigated. Anodization technique was used to fabricate porous silicon photodetector at 10 mA/cm<sup>2</sup> for 10 min. The structural, morphological, and photoluminescence properties of porous silicon and gold nanoparticles were investigated. Dark and illuminated current–voltage I–V characteristics, linearity, spectral responsivity, detectivity, and pulsed responsivity of photodetector were investigated before and after RTO and after incorporation of gold nanoparticles. The photosensitivity of nano-porous silicon photodetector at 365 nm was increased from 44 to 154 mA/W and to 200 mA/W at 10 V bias after RTO process and incorporating the gold nanoparticles into the silicon matrix, respectively.

**Keywords** Porous silicon · RTO · Embedding · Gold nanoparticles

## Introduction

Ultraviolet detectors are of great importance due to their many industrial applications, such as semiconductor devices processing, missiles plume detection, space communication, nuclear reactor, and ozone monitoring (Min and Kang 2001; Monroy et al. 2001, 2003). Wide band-gap compound semiconducting materials, such as diamond, SiC, GaN, and

AlGaN, were widely used to fabricate high sensitivity UV detectors (Jain et al. 2000; Nanishi et al. 2003; Sang et al. 2013); these detectors are expensive and need sophisticated fabrication technology. Wide band-gap heterojunction detectors-based silicon have been developed to detect UV radiation, but because the mismatch in lattice constants between the overlay layer and silicon substrate had affecting negatively the photosensitivity of these photodetectors (Ding et al. 2015; Ismail 2006). Porous silicon photodetector was used for UV detection, it has many advantages over the other materials, such as high absorption coefficient for UV region, it does not require anti-reflective coating and low cost, and needs simple fabrication technology (Berger et al. 1994; Ismail 2010). The reported data revealed that the preparation conditions like pore size, porosity, and pore structure play major role in enhancement of its photosensitivity for UV region. Recently, Lin et al. (2013) reported the enhancement of nano-porous silicon photodetector for UV region by rapid thermal oxidation RTO technique, the photosensitivity has been increased from 14 to 130 mA/W at 350 nm after RTO. In this work, synthesis and performance improvement of anodized nano-porous silicon detectors for UV region by post-rapid thermal oxidation and embedding of gold nanoparticles into silicon matrix were investigated and analyzed.

## Experiment

Mirror-like monocrystalline Si substrates of 350 μm thick, 1–3 Ω cm electrical resistivity, and (111) orientations were used. The porous layer was prepared by electrochemical etching technique. The substrates were cut into rectangles of (1 cm × 1 cm) areas. Anodization was carried out using a Teflon cell with an electrolyte containing 48% HF and 99.9%

✉ Raid A. Ismail  
raidismail@yahoo.com

<sup>1</sup> Department of Applied Science, University of Technology, Baghdad, Iraq

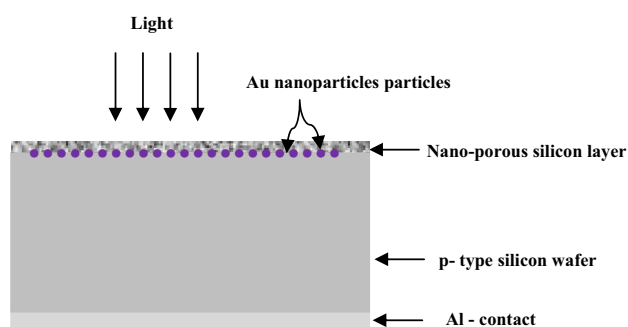


**Fig. 1** Schematic diagram of Au nanoparticles incorporated nano-porous silicon photodetector

ethanol 1:1 by volume. The silicon samples were anodized at current density of  $10 \text{ mA/cm}^2$  for 10 min. After anodization, the silicon samples were washed out with deionized water for 15 min and dried under  $\text{N}_2$  ambient. RTO system was used to oxidize the porous silicon layer at  $700 \text{ }^\circ\text{C}$  for 90 s in static air using bank of halogen lamps with one-side illumination. Pulsed laser ablation technique was used to synthesise gold nanoparticles by irradiating of high purity gold plate in methanol solution by Nd:YAG laser pulses of  $25 \text{ J/cm}^2$  laser fluence; the detail of synthesis method was presented elsewhere (Ismail et al. 2012). Incorporating the porous silicon samples with Au nanoparticles was carried out using the drop casting technique after 1 h of sonication. After drop casing, the samples were heated at  $60 \text{ }^\circ\text{C}$  under nitrogen, Fig. 1 shows a sketch of cross-sectional view of Au nanoparticles embedded nano-porous silicon photodetector. Structural, morphological, and optical properties of porous silicon and Au nanoparticles were examined by Inspect S50/FEI company scanning electron microscopy, Angstrom AA 300 atomic force microscopy, photoluminescence spectrometer (Liconix 3205N), and Shimadzu UV–Vis spectrophotometer. The dark and illuminated I–V characteristics of photodetectors were investigated; the photocurrent of the photodetectors was estimated under white light and UV source (365 nm) illumination. The spectral responsivity of the photodetectors before and after RTO and incorporation with Au nanoparticles was measured in the range of 350–900 nm using a monochromator. To calibrate the monochromator, Sanwa silicon power meter was used for this purpose. All the above characteristics were investigated at room temperature. Pulsed responsivity was measured in the absence of external bias using pulsed UV source at  $\lambda = 365 \text{ nm}$  and storage oscilloscope of 200 MHz bandwidth.

## Results and discussion

Figure 2 shows the SEM image of porous silicon before and after RTO process, it is clear that the pores were uniform distributed and almost have semi-circular shape with average size of 200 nm. The porosity was estimated

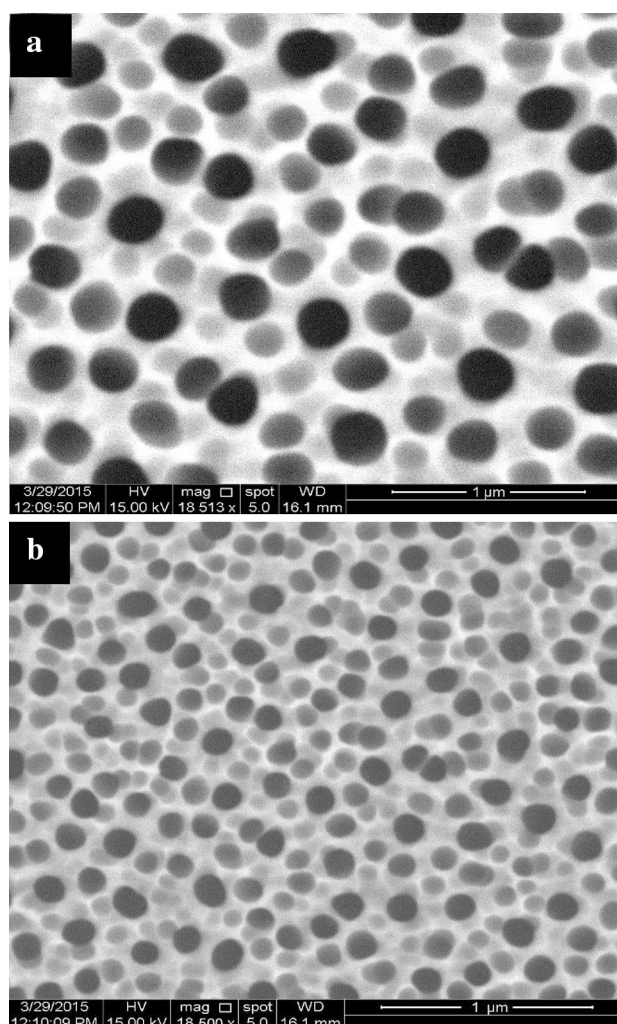


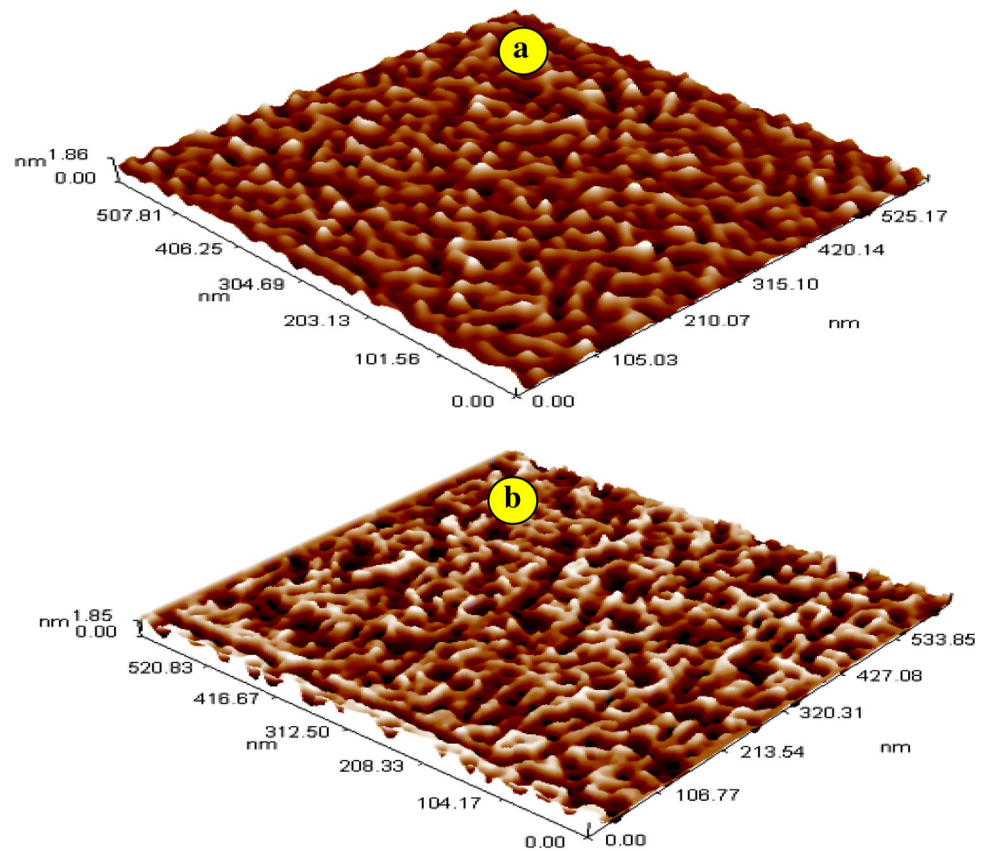
**Fig. 2** SEM images of as-prepared (a) and oxidized porous silicon (b)

and was about 80%. After oxidation, the average pore size decreased to 85 nm and no significant alteration in pore structure was noticed; the wall size was found to be around 33 nm.

The 3D AFM images of as-formed and oxidized porous silicon layers are given in Fig. 3, AFM image of as-prepared porous silicon (Fig. 3a) exhibits pyramid-like shape distributed randomly over the whole porous surface. The root mean square, RMS, of surface roughness and particles height are decreased after RTO. The morphology of porous layer was changed remarkably after RTO process, as shown in Fig. 3b, the pores boundaries became clear, and also this figure confirms that the pores have relatively different sizes and shapes. The thickness of pore wall was also increased after RTO. The estimated average particles' size of porous layer before and after RTO was 50 and 25 nm, respectively.

The PL spectra of as-prepared porous silicon, oxidized porous silicon, and Au embedded porous silicon are

**Fig. 3** AFM images of porous silicon surface before (a) and after RTO (b)



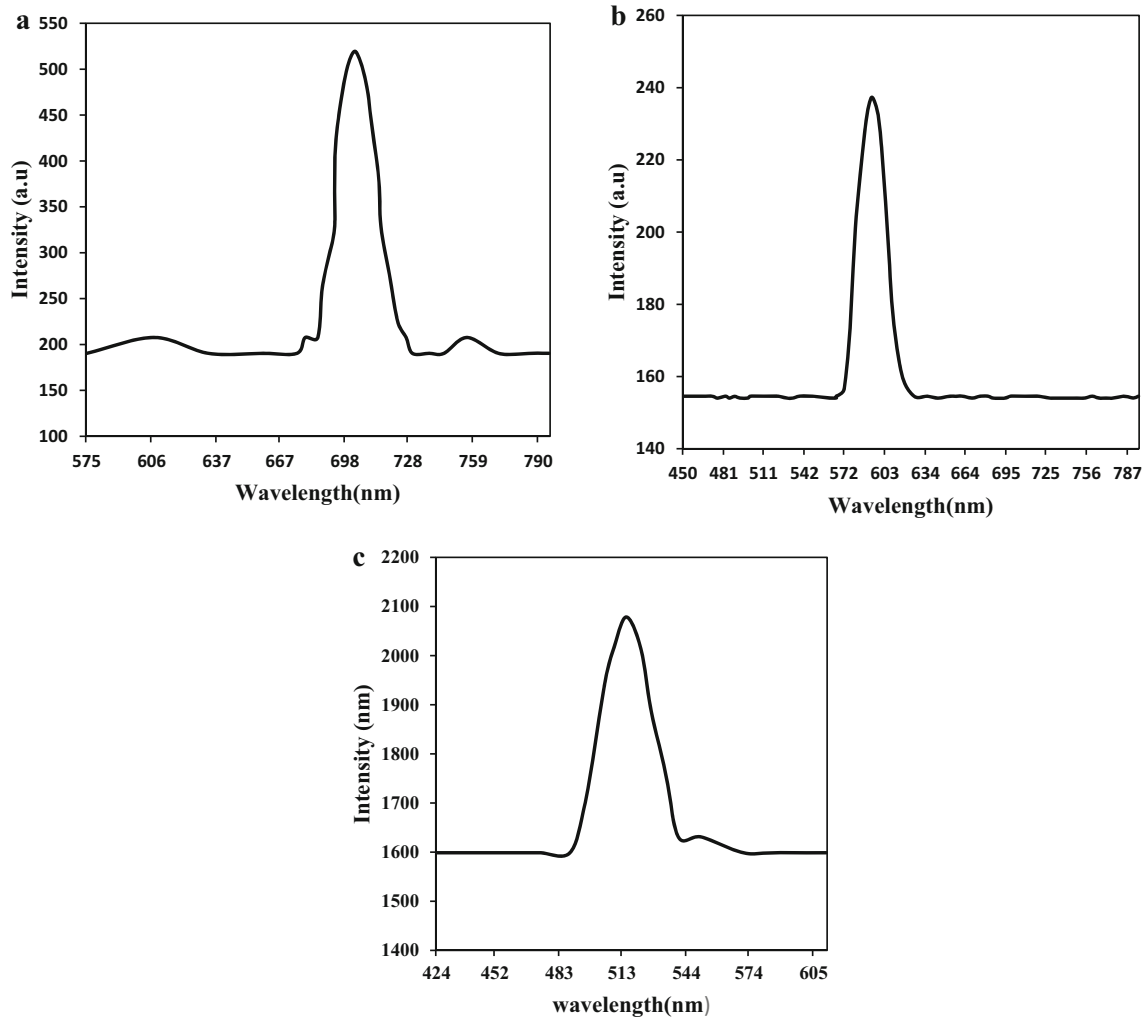
demonstrated in Fig. 4. The PL spectrum of as-prepared porous silicon revealed that the peak intensity centred at 703 nm corresponding to energy of 1.76 eV and the PL of oxidized porous sample exhibits the maximum intensity at 593 nm which corresponds to energy of 2.09 eV. The shift in PL peak of oxidized sample toward short wavelengths (blue shift of 110 nm) can be ascribed to reduction of thickness silicon layer and due to decreasing of effective silicon nanosized by oxidation (Song et al. 1997; Elhouichet and Oueslati 2002). The PL spectrum of Au embedded porous silicon revealed that PL peak was shifted to 515 nm (blue shift of 188 nm) which corresponded to green light region as well as the PL intensity has been increased after this embedding. The origin of blue shift can be ascribed to surface plasmon resonance SPR; this result agrees with results reported by Tengku et al. (2013). The full width at half maximum, FWHM, of porous PL spectrum was increased after Au embedding. This useful shift in PL after RTO and after embedding of Au nanoparticles can enhance the spectral detection of porous silicon photodetectors towards the short wavelengths.

Figure 5 shows the absorbance spectra of colloidal Au nanoparticles; it is obvious that there are two noticeable absorption peaks located at 302 and 500 nm due to quantum confinement indicating the formation Au nanoparticles (Tengku et al. 2013). The Au colloidal nanoparticles

solution was found to have a pink color. The morphology of Au nanoparticles which investigated using the AFM technique is given in Fig. 6; it has seen that all the particles were vertically oriented. The average particles size estimated from this measurement was around 45 nm. The SEM image of Au nanoparticles deposited on porous silicon was illustrated in Fig. 7; the agglomeration of Au nanoparticles to form micro-sized particles with different shapes was noticed as shown in the inset of Fig. 7. Most of coarse Au particles are agglomerated at silicon walls and the nanosized Au particles are entered inside the pores of silicon.

The EDX spectrum of Au nanoparticles deposited on porous silicon is presented in Fig. 8, this figure confirmed the presence of Au particles, silicon, and oxygen. The silicon peak in EDX arises from the molecules of oxygen trapped in pores. No traces of other elements were found in the EDX spectrum.

The effect of Au nanoparticles embedded and oxidation on the dark current–voltage characteristics of porous silicon photodetectors are depicted in Fig. 9; the quality of junction was significantly improved after adding of Au nanoparticles. The incorporation of Au nanoparticles resulted in increasing the forward current and decreasing the leakage current due to decreasing the resistivity of porous layer. No remarkable variation in the I–V



**Fig. 4** PL spectra of as-prepared porous silicon surface (a) after RTO (b) after Au nanoparticles embedding (c)

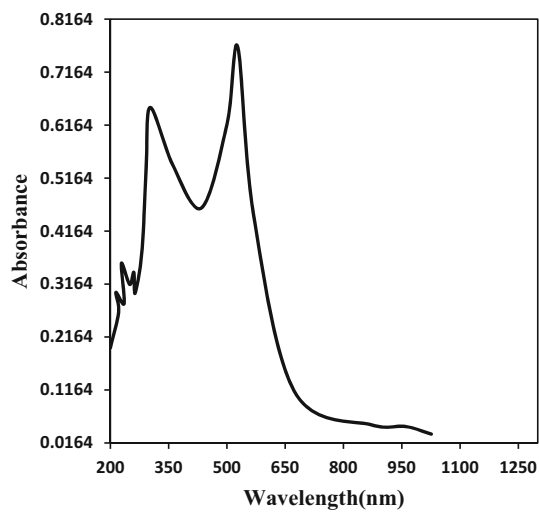


**Fig. 5** Absorbance of colloidal Au nanoparticles

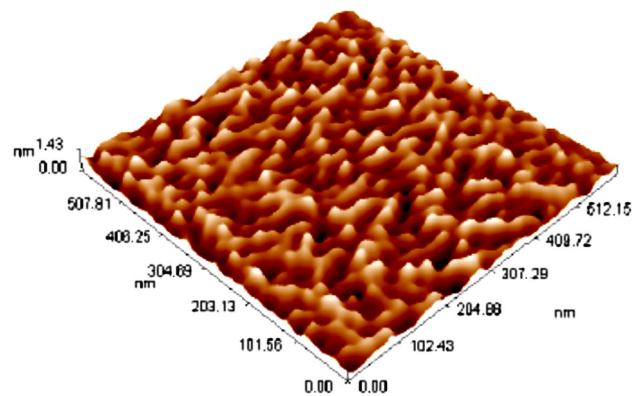


**Fig. 6** 3D AFM image of Au nanoparticles

characteristics of photodetector was seen after RTO process; slight decreasing in forward current can be ascribed to increasing of resistivity due to oxidation cycle. The recti-

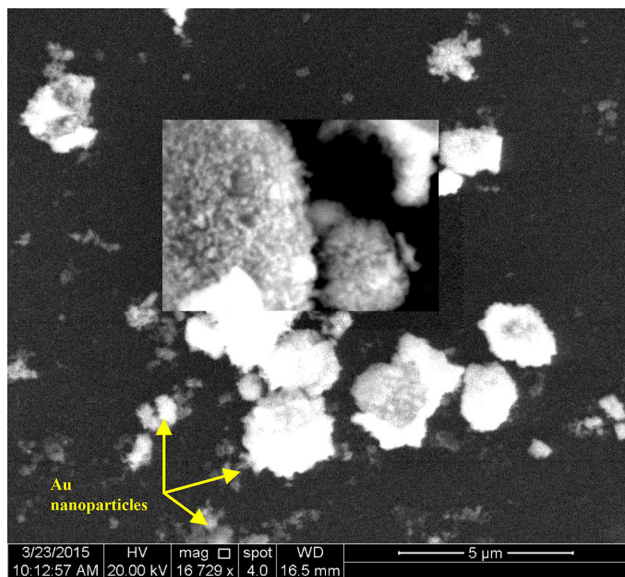


Fig. 7 SEM image of Au embedded in silicon matrix

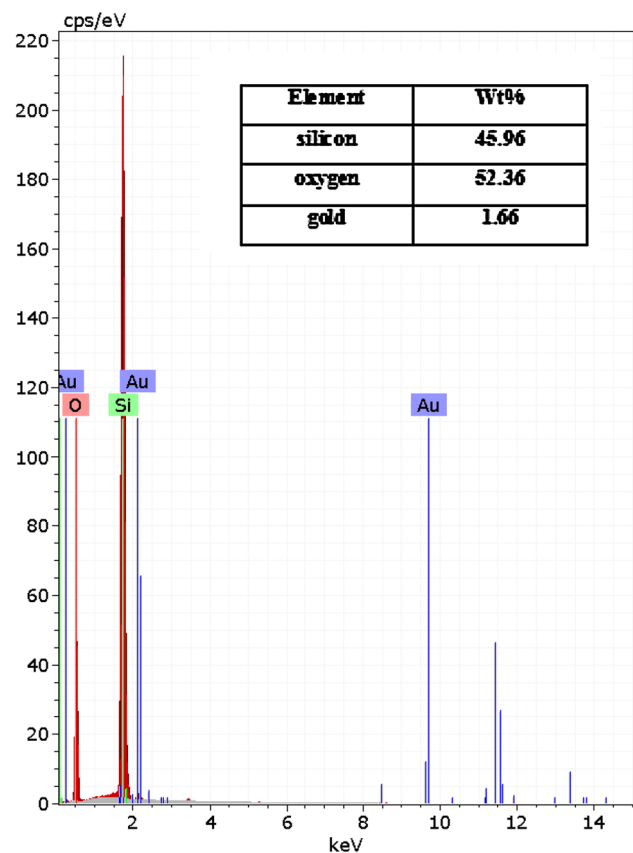


Fig. 8 EDX spectrum of Au nanoparticles embedded in silicon matrix

fication factor (ratio of forward current to reverse current  $I_f/I_r$ ) of Au embedded porous silicon junction was higher than the as-formed and oxidizing nano-porous silicon junctions. No soft breakdown voltage was noticed at bias

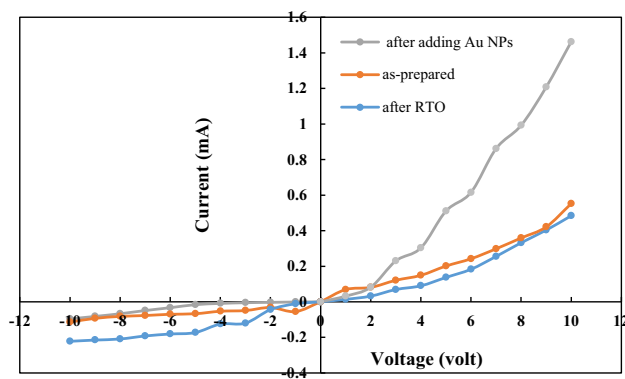


Fig. 9 Dark I–V characteristics of porous silicon photodetectors

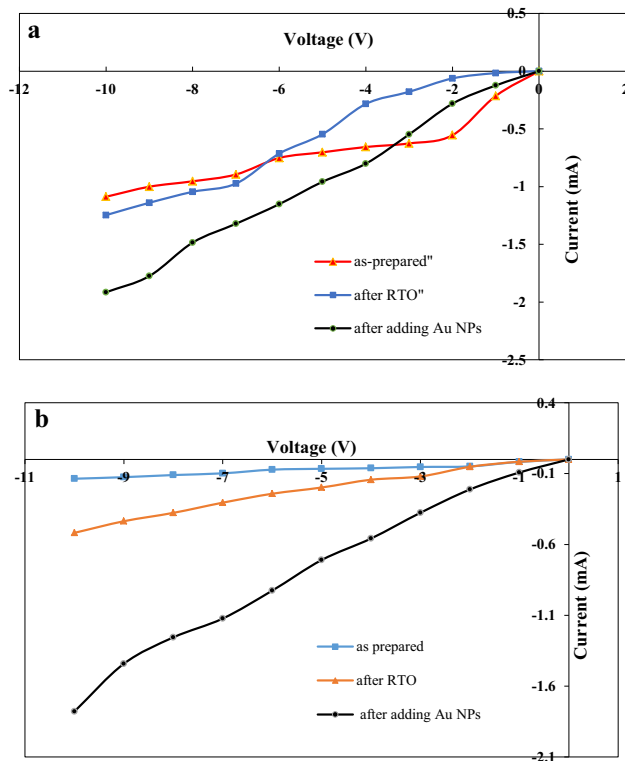
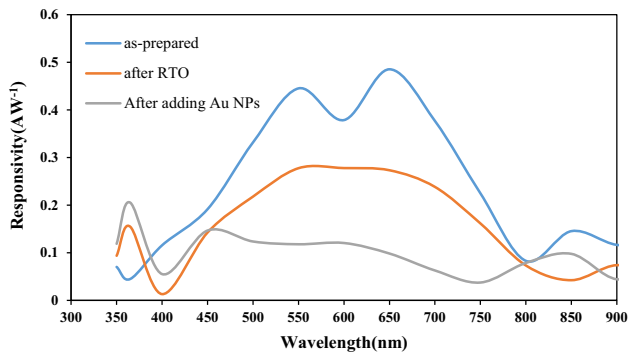


Fig. 10 I–V characteristics of photodetectors under illumination with a white light and b UV light

<10 V. It is clearly seen that the reverse current was decreased after Au embedding and became bias independent. The ideality factor  $n$  of porous silicon junction was calculated using the following equation and has found its value was 5.1, 6, and 2.8 for as-prepared junction, oxidized junction, and Au embedded junction, respectively:

$$n = \frac{q}{kT} \frac{\Delta V}{\Delta \ln \frac{I_f}{I_s}} \quad (1)$$

where  $I_s$  is saturation current of the junction which calculated from a semi-logarithmic relationship of forward



**Fig. 11** Spectral responsivity plot of porous silicon photodetectors at 10 V bias

current versus bias voltage plot (not shown here). Decreasing the ideality factor after adding Au particles in silicon matrix indicating an improvement in junction performance arises from decreasing of structural defects and due to decreasing the shunt resistance of porous layer.

Figure 10 shows the I–V characteristics of as-prepared, Au embedded, and oxidized porous silicon photodetectors under white light and UV illumination. The photocurrent  $I_{ph}$  has increased under white illumination from 1.08 to 1.24 and to 1.91 mA at 10 V bias after RTO and Au embedding, respectively. This improvement can be attributed to reduction in surface states and recombination centres. The on/off ratio ( $I_{ph}/I_d$  ratio) at 10 V of as-prepared

oxidized and Au embedded porous silicon photodetectors at 365 nm illumination was found to be 1.3, 5.1, and 8.1, respectively. This enhancement could be attributed to increasing the absorption coefficient of porous layer and short diffusion length of photogenerated carriers, as well as due to increasing the photo-induced carriers from Au to porous silicon. The spectral responsivity plot at 10 V bias of porous silicon photodetectors is given in Fig. 11, the peak of response of as-prepared and oxidized photodetectors was found at visible region, while the peak of response of Au nanoparticles embedded porous silicon photodetector was located at 365 nm with responsivity of 205 mA/W due to increasing the light absorption by Au nanoparticles. This value is higher than that enhanced p–n junction silicon photodiodes and wide band-gap heterojunction-based silicon photodetectors (Khodami et al. 2008; Han et al. 2015; Um et al. 2011). The shift in peak of response of photodetector toward UV region after adding the Au nanoparticles ascribed to the enhancement in UV absorption by Au nanoparticles agglomerated at silicon surface. Decreasing of the responsivity after 750 nm is due to absorption edge of porous silicon.

The pulsed responsivity of photodetectors at 365 nm has been investigated, as shown in Fig. 12. The pulsed responsivity of as-prepared porous silicon photodetector has increased from 1.3 to 1.7 V/W and to 2 V/W at zero bias after oxidizing and adding of Au nanoparticles,

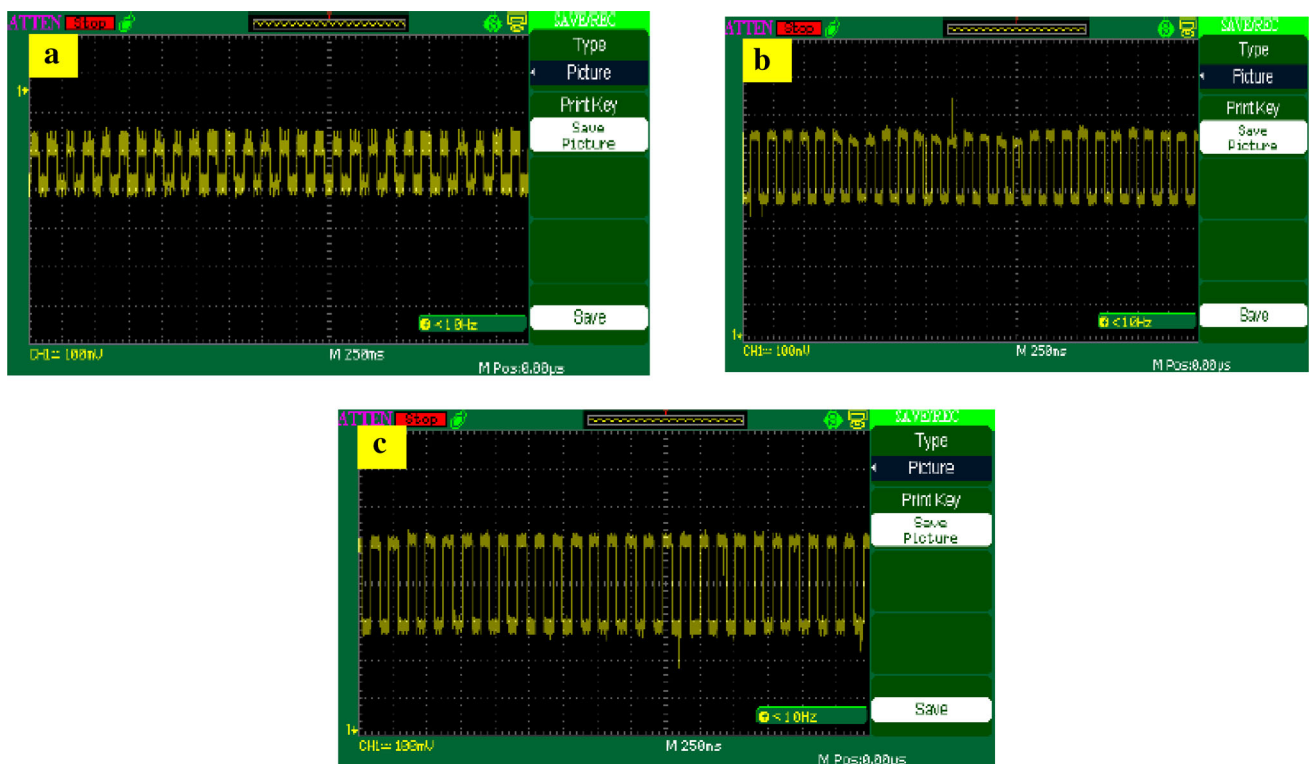


**Fig. 12** Pulse response of porous photodetectors (a) as-prepared (b) after RTO (c) after Au nanoparticles embedding (c)

respectively, indicating the improvement in UV photoreponse of the porous silicon photodetector.

This result can be explained on the basis of increasing the depletion layer width of the junction after RTO and embedding of Au nanoparticles.

## Conclusion

In this paper, we have successfully enhanced the sensitivity of porous silicon photodetectors for UV detection using simple, competitive, cost-effective, and novel technique. This technique involved two steps: post-rapid thermal oxidation of porous silicon photodetector and incorporation of gold nanoparticles into silicon matrix photodetector. The rectification properties of junction have been improved after adding of Au nanoparticles. The on/off ratio of photodetectors under reverse bias was increased after oxidation and embedding steps. The Au nanoparticles embedded porous silicon photodetector has a peak of response at 365 nm with sensitivity higher than as-prepared and oxidized nano-porous silicon photodetectors by factor 4.6 and 1.6, respectively. The pulsed responsivity of photodetectors for UV light has improved after post RTO of porous layer and embedding of Au nanoparticles into pores of silicon matrix.

**Open Access** This article is distributed under the terms of the Creative Commons Attribution 4.0 International License (<http://creativecommons.org/licenses/by/4.0/>), which permits unrestricted use, distribution, and reproduction in any medium, provided you give appropriate credit to the original author(s) and the source, provide a link to the Creative Commons license, and indicate if changes were made.

## References

Berger M, Dieker C, Thonissen M, Vescan L, Luth H, Munder H, Theiss W, Wernke M, Grosse P (1994) Porosity superlattices: a new class of Si heterostructures. *J Phys D Appl Phys* 27:1333

- Ding M, Zhao D, Yao B, Li Z, Xu X (2015) Ultraviolet photodetector based on heterojunction of n-ZnO microwire/p-GaN film. *RSC Adv* 5:908
- Elhouichet H, Oueslati M (2002) The role of ambient ageing on porous silicon photoluminescence: evidence of phonon contribution. *Appl Surf Sci* 191:11
- Han W, Xiang-Liang J, Chang-Ping C, Man-Fang T, Ke-Han Z (2015) A novel integrated ultraviolet photodetector based on standard CMOS process. *Chin Phys B* 24:038501
- Ismail R (2006) Fabrication and characteristics study of n-Bi<sub>2</sub>O<sub>3</sub>/n-Si heterojunction. *J Semicond Technol Sci* 6:119
- Ismail R (2010) Fabrication and characterization of photodetector based on porous silicon. *e-J Surf Sci Nanotechnol* 8:388
- Ismail R, Ali A, Hasson K (2012) Characteristics of a silicon Schottky photodetector produced from colloidal gold nanoparticles. *Micro Nano Lett* 7:536
- Jain S, Narayan J, Overstraeten R (2000) III-nitrides: growth, characterization, and properties. *J Appl Phys* 87:965
- Khodami I, Taghibakhsh F, Karim KS (2008) UV-enhanced a-Si: H metal-semiconductor-metal photodetector. *IEEE Electron Device Lett* 29:1007
- Lin M, Lin Y, Wu K, Huang C (2013) Preparation of oxidized nanoporous-silicon thin films for ultra-violet optical-sensing applications. *Thin Solid Films* 529:275
- Nam-Ki Min, Chul-Goo Kang, Suk-In Hong (2001) Static and transient characteristics of Si: Au-Based V-Groove P-I-N Photodetectors. *J Korean Phys Soc* 39:62
- Monroy E, Calle F, Pau JL, Munoz E, Omnes F, Beaumont B, Gibart P (2001) AlGaIn-based UV photodetectors. *J Cryst Growth* 230:537
- Monroy E, Omnes F, Calle F (2003) Wide-bandgap semiconductor ultraviolet photodetectors. *Semicond Sci Technol* 18:R33
- Nanishi Y, Saito Y, Yamaguchi T (2003) RF-molecular beam epitaxy growth and properties of InN and related alloys. *Jpn J Appl Phys* 42:2549
- Sang L, Liao M, Sumiya M (2013) A comprehensive review of semiconductor ultraviolet photodetectors: from thin film to one-dimensional nanostructures. *Sensors* 13:10482
- Song H, Qin G, Yao D, Chen Z, Bao X (1997) Microsecond photoluminescence. *Solid State Commun* 102:813
- Tengku T, Hashim M, Ali N, Yazid H, Adnan R (2013) Optical absorption and photoluminescence studies of gold nanoparticles deposited on porous silicon. *Nanoscale Res Lett* 8:35
- Um H, Moiz S, Park K, Jung J, Jee S, Ahn C, Kim D, Cho H, Kim D, Lee J (2011) Highly selective spectral response with enhanced responsivity of n-ZnO/p-Si radial heterojunction nanowire photodiodes. *Appl Phys Lett* 98:33102